Available online at www.sciencedirect.com
SCIENCE DIRECT®
Organic Electronics 5 (2004) 237–249
Organic Electronics
www.elsevier.com/locate/orgel

Consequences of twisting the aromatic core of *N*,*N*′-dimethylperylene-3,4,9,10-biscarboximide by chemical substitution for the electronic coupling and electric transport in thin films

Harald Graaf [a,b,1], Wilfried Michaelis [a,b], Günter Schnurpfeil [b], Nils Jaeger [b], Derck Schlettwein [a,b,*]

[a] *School of Mathematics and Natural Sciences, University of Oldenburg, P.O. Box 2503, D-26111 Oldenburg, Germany*
[b] *Department of Chemistry, University of Bremen, 28334 Bremen, Germany*

Received 8 July 2003; received in revised form 4 January 2004; accepted 14 February 2004
Available online 12 April 2004

Abstract

Thin films of 1,6,7,12-tetrachloro-*N*,*N*′-dimethylperylene-3,4,9,10-biscarboximide (Cl_4MePTCDI) prepared by physical vapor deposition (PVD) were compared to thin films of the unchlorinated *N*,*N*′-dimethylperylene-3,4,9,10-biscarboximide (MePTCDI) to investigate the influence of a changed molecular structure on the electrical properties of the materials. The films were prepared on microstructured Si/SiO_2 substrates with interdigitated Au electrode arrays of 2 μm electrode distance or on quartz glass with electrode distances in the mm range. The films were investigated by conductance measurements, thermoelectric power, electric field effect, ultraviolet photoelectron spectroscopy (UPS) and atomic force microscopy (AFM). The thickness-dependence of the conductance measured during film growth (in situ) indicated a growth mode in islands (Volmer-Weber), which was confirmed by subsequent AFM. As expected, Cl_4MePTCDI was characterized as an organic n-type semiconductor. Charge transport occurred by a hopping mechanism as revealed by temperature-dependent thermopower and field-effect measurements. Effective electron mobilities at room temperature were found around 10^{-5} $cm^2\,V^{-1}\,s^{-1}$ considerably lower than the values for MePTCDI. A rather constant concentration of mobile electrons of $(1–2)\times10^{18}$ cm^{-3} was determined for both materials. The morphology of Cl_4MePTCDI islands indicated amorphous growth as opposed to crystals obtained for MePTCDI, as also revealed earlier by optical spectroscopy and the role of crystallinity in the electrical conduction is discussed.

* Corresponding author. Address: Institute of Applied Physics, Justus-Liebig-University Giessen, Heinrich-Buff-Ring 16, D-35392 Giessen, Germany. Tel.: +49-641-99-33400/33401; fax: +49-641-99-33409.
E-mail address: schlettwein@uni-giessen.de (D. Schlettwein).
[1] Present address: Institute of Physics, Chemnitz University of Technology, 09107 Chemnitz, Germany.

1566-1199/$ - see front matter © 2004 Elsevier B.V. All rights reserved.
doi:10.1016/j.orgel.2004.02.003

PACS: 68.55.Jk; 72.80.Le; 73.50.Gr; 73.61.Ph
Keywords: Organic semiconductor; Perylene pigment; Field effect; Seebeck coefficient; Mobility; Hopping transport

1. Introduction

Intermolecular coupling in thin films of organic semiconductors can be considered a key element that determines their optical and electrical properties. This group of materials is of considerable interest for fundamental research, as well as in view of realized or prospective technical applications. Electrophotography as an established technology, e.g., uses organic pigments as photoconductors in the charge-generation layers. Organic light emitting diodes (OLED), an emerging technology of displays, are based on the emission from an electrically induced excited state of molecular materials. Organic semiconductors could also be shown to work as ambipolar field-effect-transistors [1] and as active components in organic photovoltaic cells [2–4]. A high level of control over the intermolecular interaction was needed to achieve these properties. From the results it became clear that an increased level of control over intermolecular coupling is also needed in the area of thin films in order to reach attractive optical and electrical characteristics [5].

Of particular interest is the variation of electrical properties when crystalline films or single crystals are compared with amorphous semiconducting films in which the co-planar interactions of the aromatic systems are blocked. As a consequence a hindered formation of excimers was observed, leading to a significantly increased luminescence in the solid state when otherwise quite similar molecules were compared [6]. The question arises, whether this decreased coupling of the aromatic systems will also be reflected in a decreased mobility of charge-carriers. In this paper thin vapor-deposited films of two different but closely related materials—the planar *N*,*N*′-dimethylperylene-3,4,9,10-biscarboximide (MePTCDI) and the twisted 1,6,7,12-tetrachloro-*N*,*N*′-dimethylperylene-3,4,9,10-biscarboximide (Cl_4MePTCDI) [7] will be investigated. To confirm the role of the chlorine substitution, some results at perylene-3,4,9,10-tetracarboxilic acid (PTCDA) and 1,6,7,12-tetrachloroperylene-3,4,9,10-tetracarboxilic acid (Cl_4PTCDA) will also be discussed.

The molecular structures of Cl_4MePTCDI and MePTCDI revealed by geometry optimization in molecular orbital calculations on the semiempirical level are shown in Fig. 1. For Cl_4MePTCDI, two possible enantiomeric structures are shown, a mixture of which has to be anticipated in the films under the given experimental conditions. The parallel arrangement of the electronic π-systems is considerably blocked as has been concluded from an optical characterization reported earlier [6]. For MePTCDI a well-defined intermolecular interaction was found, which led to a strong chromophore coupling and a splitting of the absorption band in the UV/vis spectra. [8] The luminescence was widely quenched due to excimer formation and subsequent non-radiative decay in the solid state. In the case of Cl_4MePTCDI no band splitting in the UV/vis-absorption spectra was found

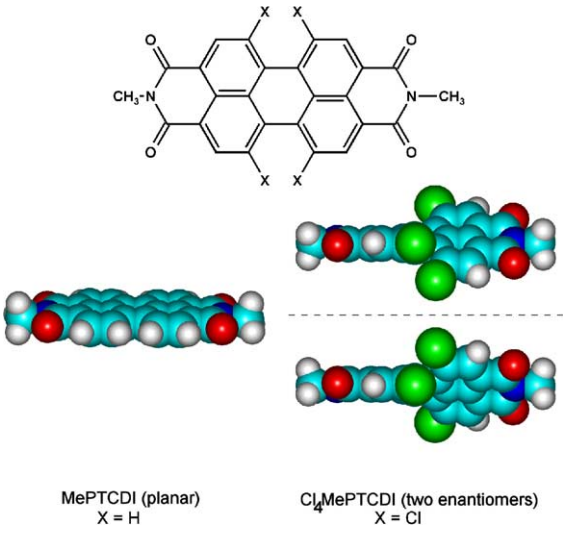

Fig. 1. Molecular structures of the investigated molecules MePTCDI and Cl_4MePTCDI.

and a high luminescence yield (up to ~60% of a comparable solution) was found, which indicated a small, non-ordered intermolecular interaction in the solid state. This difference in the structure of the two solids was caused by the twisted structure of the molecule following the introduction of the four chlorine atoms. This hindered the stacking of molecules, which had also been observed for the octa-chlorinated Cl_8MePTCDI, where a crystalline structure was only found with intercalated benzene. [9] We report here on the electrical characterization of MePTCDI and Cl_4MePTCDI and discuss the influence of the chemical substitution on the film growth, electrical conductivity, charge-carrier mobility and charge-carrier concentration.

2. Experimental

MePTCDI was provided by Hoechst, Cl_4MePTCDI was synthesized as described earlier [7]. Both materials were purified by a three zone-sublimation in a quartz tube at about 1×10^{-7} mbar (Lindberg, USA). The central zone with the sample in a BN crucible boat was heated until sublimation of the purified material in the adjacent, non-heated collection zones was observed. Mass spectra of the sublimed materials showed no detectable impurities for MePTCDI and less then 0.1% Cl_5MePTCDI without any other impurities for Cl_4MePTCDI. As substrates for thermoelectric power measurements quartz glass (Westdeutsche Quarzschmelze) with two evaporated 80 nm thick gold electrodes (Balzer 99.99%) was used, probing the organic sample along a channel of 13 mm width and 10 mm length along the substrate and temperature gradient. For the conductance and field-effect measurements microstructured interdigitated gold electrode arrays on silicon dioxide with an electrode distance of 2 μm were used. A highly doped silicon layer below the SiO_2 dielectric layer was used as a resistive heater and also as the gate electrode for field-effect measurements. The small heating voltage (max. 0.5 V for 500 K) did not significantly alter the gate voltage (0, 5, 10, 15, 20, 25 and 30 V). Details of the substrate and its preparation were described elsewhere [10,11]. For the electrical measurements (field-effect and thermoelectric power) two different high vacuum systems were used as described earlier [12,13]. Before film preparation the chambers were evacuated for at least 24 h at about 350 K and the crucibles with the organic materials were kept at about 370 K. Thin films of the organic materials were deposited in situ by physical vapor deposition from resistively heated BN crucibles and the deposited mass was monitored by changes in the resonance frequency of a calibrated quartz crystal microbalance (QCM). The average film thickness was calculated based on an estimated density of 1.5 $g\,cm^{-3}$, typical for this group of materials. An equivalent of the first 50 nm of the evaporated material was not used for film preparation to ensure the highest available sample purity of the studied films. The electrical characterization was done during film growth and subsequently, without breaking the vacuum. The morphology of the films was studied at ambient conditions by atomic force microscopy (AFM), using standard Si tips in the resonant mode of a SMENA A microscope (NT-MDT) after finishing the electrical measurement. Ultraviolet photoelectron spectroscopy was performed at thin films of the materials deposited on atomically clean Au and Ag sheets (Goodfellows) by use of a VG Escalab Mark II (for MePTCDI) or a Kratos AXIS (for Cl_4MePTCDI) as installed at the LESSA facility of the chemistry department of the University of Arizona. The spectrometers were calibrated and a constant electrochemical potential of 4.0_9 eV could be assumed. The kinetic energy of photoemitted electrons was measured assuming electrical equilibrium between the metal substrate and the spectrometer with the common Fermi edge $E_{F,m}$ defined as zero. The binding energy E_B was measured relative to this level. Binding energies relative to a free electron in vacuum at infinite distance were calculated as $E_{B\infty} = E_B + 4.09$ eV to allow comparisons between different materials on an absolute scale and also with calculated values. These methods were established earlier and reported in detail [14].

Molecular orbital (MO) calculations on the semiempirical level were performed on geometry-optimized individual molecules (up to an energy gradient of less than 10^{-4} kcal $mol^{-1}\,A^{-1}$) using the PM3 parameter set as implemented in Hyperchem

5 (Hypercube Inc.). No compression or expansion of the energy scale was applied when the calculated values were compared to experimental data.

3. Results and discussion

The hindrance in aggregation of the molecules detected in the optical analysis [8] was also reflected in a smaller lattice energy of the solids leading to a decrease in the sublimation temperature from ~490 K for MePTCDI to ~400 K for Cl_4MePTCDI, observed at 5×10^{-8} mbar and an increased solubility of more than 10^{-2} mol/L for Cl_4MePTCDI in different solvents like CH_2Cl_2 as opposed to a solubility of less than 10^{-5} mol/L for MePTCDI. The twist of the molecular plane is seen as the main reason for this weaker intermolecular interaction. To which extend a possible interaction of Cl atoms of adjacent molecules may partly compensate the weaker interaction of the aromatic cores cannot be decided at present.

3.1. Electrical characterization during film growth

Evaporation of Cl_4MePTCDI onto quartz glass substrates led to the growth of islands (Volmer-Weber growth mode). This was detected in the thickness-dependence of the conductance (Fig. 2) and by AFM analysis (Fig. 3). Up to a deposited amount corresponding to an average film thickness of 45 nm no current was detected since only isolated islands of the evaporated material were formed without sufficient contact to each other to form a conductive pathway connecting the two Au electrodes. This conclusion is clearly confirmed by the AFM analysis of a film of 30 nm average thickness (Fig. 3(a)) which shows separated lentil-like islands of Cl_4MePTCDI. Above 45 nm average film thickness the current increased following a power law with an exponent close to two. Such a behavior is characteristic for the percolation of islands and hence the formation of conductive pathways in the film [8].

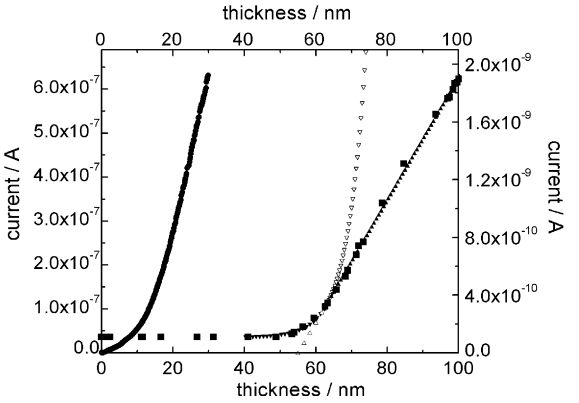

Fig. 2. In situ current measurement during evaporation of Cl_4MePTCDI on microstructured substrates (Au electrode distance 2 μm) at 318 K and an applied electric field of 500 V cm^{-1} (●) and on quartz glass (Au electrode distance 1 cm) at 313 K and an applied electric field of 10 V cm^{-1} (■). Fits to the quadratic increase (▽) and to the linear increase (△) of the current are included. Solid symbols are used where the fits are relevant, open symbols show the hypothetical further plot of the different fits beyond their range of relevance.

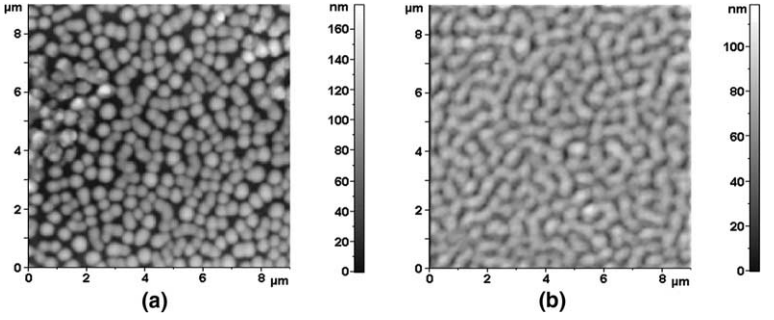

Fig. 3. AFM images of two films of Cl_4MePTCDI on glass substrate with different average film thickness. (a) 30 nm average film thickness prepared at 318 K, and (b) 70 nm average film thickness prepared at 393 K. Both samples were annealed for several hours in vacuum.

The formation of additional pathways was finished at an average film thickness of 65 nm. Above 65 nm a linear increase of the current with the deposited amount was found which is indicative of a three-dimensional growth of the conductive pathways. This finding is again in good agreement with the direct morphological analysis by AFM, since a widely closed film structure was detected for a film with 70 nm average thickness (Fig. 3(b)). A qualitatively similar behavior was found for films of MePTCDI on these substrates. Here the increase of the current started at about 30 nm and the linear regime was reached at about 80 nm average film thickness [8]. The formation of pathways at lower average film thickness for MePTCDI compared with Cl_4MePTCDI as well as the transition to the linear regime at higher average film thickness can be understood by the analysis of the morphology of the islands that are formed for the two materials. The islands of MePTCDI consist of needle-shaped particles [12] whereas Cl_4MePTCDI was deposited in lentil-shaped structures of 150 nm average height and 550 nm average diameter (Fig. 3). For the same evaporated amount of material the average length of a needle is larger than the diameter of a round lentil-like structure, i.e., an electrical pathway can be established for a lower amount of evaporated material. On the other hand more material is needed to form an almost closed layer in the case of needles that are stacked in random directions as compared to lentils with the long axis parallel to the substrate.

In spite of the differences in the molecular structure and the decreased lattice energy in the case of Cl_4MePTCDI when compared to MePTCDI, both studied materials show a growth in islands when deposited on SiO_2. This finding indicates that the intermolecular interaction of the molecules of Cl_4MePTCDI was still higher compared with the molecule–substrate interaction. The round, flat features found for Cl_4MePTCDI are consistent with an amorphous structure of the particles as concluded earlier from the optical analysis [6]. For MePTCDI, on the other hand, needle-shaped particles of well-defined morphology were formed pointing towards a crystalline structure, also consistent with the strong chromophore coupling and almost complete quenching of the luminescence reported earlier [6,12].

During the deposition on the micro- structured substrates with their considerably smaller electrode distance (2 μm) a similar qualitative behavior was observed when compared with the results on the quartz glass slides with an electrode distance of 10 mm. However, due to the smaller electrode gap and hence a decreased minimum length of conductive pathways required to observe a net charge flow, the current showed an increase that began at a considerably lower average film thickness. An increase due to first conductive pathways could now be observed starting at 1–4 nm average film thickness of Cl_4MePTCDI or at 4–5 nm of MePTCDI. Already at about 10–15 nm the current increased linearly with the amount of material, indicating that the formation of pathways was finished and that three-dimensional growth started.

3.2. Position of energy levels

Photoelectron spectroscopy following excitation in the far UV ($He_I = 21.2$ eV) is a suitable method (UPS) to investigate the position of occupied electronic levels in organic thin films prepared under vacuum conditions without intermediate contact to ambient atmosphere [14–17]. Fig. 4(a) shows a direct comparison of the spectra obtained at thin films of Cl_4MePTCDI and MePTCDI showing the binding energies of the electrons in the film relative to an electron in vacuum independent from the sample ($E_{B\infty}$). For Cl_4MePTCDI a shift of the emissions in the HOMO range (low binding energies) towards higher binding energies is observed. This finding is confirmed by semi-empirical molecular orbital calculations for the individual molecules, shown in Fig. 4(b). This observed trend is expected by a stabilization of the electronic levels due to the electron-withdrawing influence of the electronegative Cl^- substituents. When the electronic structure of MePTCDI was optimized in the molecular structure of Cl_4MePTCDI (replacement of Cl by H, geometry optimization only of these H atoms), the

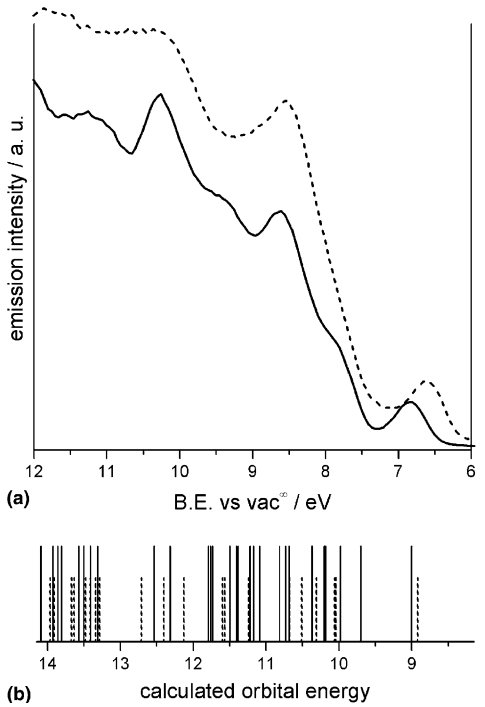

Fig. 4. Ultraviolet photoelectron spectra (a, excitation by He_I, 21.2 eV) of Cl_4MePTCDI (—) and MePTCDI (----) vapor-deposited (~4 nm) on polycrystalline Au and semiempirical calculated orbital energies (b, PM3 parameter set). The calculated energy values were not compressed or expanded on the energy scale, but the scale is shifted relative to the experimental scale as indicated in the figure.

MePTCDI HOMO was destabilized by only 0.002 eV. It was thereby shown that for the position of molecular energy levels the electronic influence of Cl dominates over the structural influence. The energy scale of the calculated values E_{calc} is shifted to give alignment of the MePTCDI HOMO position as seen on the axes to allow direct comparisons between the calculated orbital energies and the experimental spectra for Cl_4MePTCDI. It should be noted that the shift of the calculated values in comparison to the experiments is smaller for Cl_4MePTCDI (2.15 eV) than for MePTCDI (2.30 eV) or PTCDA (2.60 eV). Not only the HOMO-positions, but also deeper-lying spectral features are predicted by the calculation. For Cl_4MePTCDI the gap towards the next-lowest lying orbital below the HOMO was calculated to be significantly smaller than for MePTCDI. This is also seen in the shoulder at 7.8 eV in the experimental spectrum for Cl_4MePTCDI when compared with MePTCDI.

In ultraviolet photoelectron spectroscopy (UPS) mainly emission from the top monolayer is observed due to the low transmission for electrons from deeper layers and a value for the bulk of the material can therefore only be estimated [14]. A distribution of binding energies arising from structural inhomogeneity in polycrystalline samples has also to be considered which further adds to the complexity of the observed experimental spectra [19]. For a number of studies the ionization energy of a material relative to its vacuum-level is relevant, therefore these values are also presented in Table 1 by measuring the onset of the spectra at low kinetic energy and calculating the value of E_i^{HOMO} for the position of the HOMO maximum (characteristic for the surface and/or the most likely structure) and E_i^{thresh} for the cutoff at low binding energy (best estimate for the ionization energy in the bulk of the materials, but possibly superimposed by structural disorder). Values of PTCDA and the calculated values for the chlorinated Cl_4PTCDA were also included for comparison purposes.

The stabilization of the electronic energy levels in Cl_4MePTCDI relative to MePTCDI is clearly seen on the different scales. Dependent upon the chosen experimental reference, however, a difference of 0.2 eV up to 0.6 eV is obtained. The HOMO position of Cl_4MePTCDI is

Table 1
Binding energies of the highest occupied molecular orbital in MePTCDI, Cl_4MePTCDI and PTCDA relative to the energy of an electron at infinite distance from the sample ($E_{B\infty}$) and the ionization energy relative to the sample vacuum level for the maximum of the emission band (E_i^{max}) and the cutoff at low binding energies (E_i^{thresh}) compared to the calculated HOMO energy E_{calc}

	$E_{B\infty}^{max}$	E_i^{max}	E_i^{thresh}	E_{calc}
MePTCDI	6.6_1	6.6_4	6.1_4	8.9_2
Cl_4Me-PTCDI	6.8_3	7.1_4	6.7_2	9.0_1
PTCDA	6.7_1	7.0_5[a]		9.3_1
Cl_4PTCDA		7.4_5[b]	6.9_4[b]	9.3_6

[a] According to [18].
[b] According to [20].

found even lower in energy than that of PTCDA. This is surprising in view of the calculated orbital energies E_{calc} which give a position for the HOMO of Cl_4MePTCDI only about 0.1 eV lower in energy than that of MePTCDI and still 0.3 eV above PTCDA. To distinguish between errors in the experiments or in the calculations, the calculation was therefore also performed for Cl_4PTCDA and showed an even smaller influence of the Cl atoms. Also in this case, however, recent experiments also showed a considerably larger shift (Table 1). A systematic difference was therefore obtained which points at a final-state effect in the UPS experiments since a good correlation of calculated values with UPS experiments was observed earlier for organic semiconductors [14,21]. Chlorination obviously leads to a decreased stabilization of the molecular cation formed during photoemission, a thereby decreased kinetic energy of the emitted photoelectrons and hence an apparently higher binding energy. Such a decreased stabilization of cations in the films may be unexpected in view of the generally high polarizability of Cl atoms but appears reasonable in view of the decreased intermolecular coupling in Cl_4MePTCDI and Cl_4PTCDA when compared with the unchlorinated molecules. This decreased intermolecular coupling was also observed in optical spectroscopy at thin films [6] and is therefore believed to over-compensate the higher polarizability of Cl atoms.

Positions for the lowest unoccupied molecular orbitals (LUMO), relevant for interactions with dopant molecules in the films since n-type conduction was observed, were calculated by adding the energy of the longest wavelength intramolecular optical transition as an estimate of the forbidden gap. The position of the LUMO for Cl_4MePTCDI was found about 0.15 eV lower than that for MePTCDI. This estimate does not account, however, for any exciton dissociation energy although that has been discussed in a number of studies now and has been determined to be around 0.4–0.5 eV based on comparisons with results of inverse photoelectron emission spectroscopy [5,19]. In optical spectra of thin films, Cl_4MePTCDI showed a considerably suppressed intermolecular coupling of the electronic systems when compared with the unsubstituted MePTCDI [6]. It therefore seems reasonable to assume a higher exciton dissociation energy for Cl_4MePTCDI due to a smaller intermolecular stabilization of ions as also concluded from the above comparison of calculated and experimental HOMO positions. Given the only slightly lower HOMO position of Cl_4MePTCDI (calc. 0.1 eV) and the size of the exciton dissociation energy of at least 0.4–0.5 eV [19], the relative LUMO positions of the two materials can not be discussed in detail but can be assumed to be rather close in energy.

3.3. Electrical properties of thin films

To probe the influence of the intermolecular interaction on the electrical conduction following film preparation, the specific conductivity σ and the charge-carrier mobility μ were determined at room temperature. To evaluate the characteristics of the mobility of charge-carriers in the films, measurements of the field-effect were carried out (Fig. 5). The current–voltage behavior was typical for devices in which the current at higher voltages

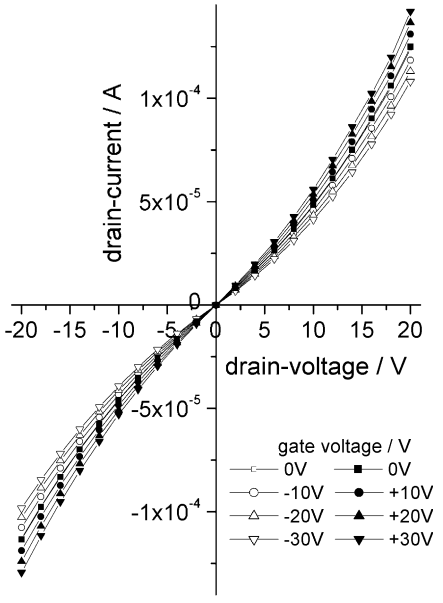

Fig. 5. Drain-current–voltage curves of a Cl_4MePTCDI film (prepared at 303 K, average film thickness 30 nm, 2 μm electrode distance) at different gate-voltages.

Table 2
Specific conductivity σ, charge-carrier mobility μ and charge-carrier concentration n as well as their temperature dependence as represented in the activation energies E_A of the specific conductivity, E_H of the hopping energy and ΔE of the charge-carrier concentration in films of Cl_4MePTCDI and MePTCDI. The growth rate r during film preparation is given for comparison purposes

Film	r/nm min^{-1}	σ/S cm^{-1}	μ/cm^2 V^{-1} s^{-1}	n/cm^{-3}	E_A/eV	E_H/eV (contribution to E_A)	ΔE/eV (contribution to E_A)
Cl_4MePTCDI (1)	0.088	1.38×10^{-6}	7.44×10^{-6}	1.15×10^{18}	0.35	0.23 (66%)	0.12 (34%)
Cl_4MePTCDI (2)	0.1	1.4×10^{-6}	–	–	0.34	0.21 (62%)	0.13 (38%)
MePTCDI (1)	0.07	1.77×10^{-4}	5.60×10^{-4}	1.97×10^{18}	0.20	0.11 (55%)	0.09 (45%)
MePTCDI (Ref. [13])	0.3	1.3×10^{-4}	–	–	0.20	0.14 (70%)	0.06 (30%)

The parameters were obtained at 303 K for films prepared at 313 K on micro-structured electrode arrays for the films (1) and for films (2) prepared on quartz glass with an electrode distance of 10 mm and which was measured at 312 K. MePTCDI (Ref. [13]) was prepared under similar conditions as Cl_4MePTCDI (2).

is limited by carrier injection. The linear characteristics at low voltage (Ohmic range) transforms into a power-law dependence with an exponent >1 (space–charge-limited current) at higher voltage. When an additional electric field was applied between the Au electrodes that are in contact with the film (source and drain electrode) and the Si electrode (gate) beneath the insulating SiO_2, the current between source and drain I_d changed significantly (field-effect). At positive gate voltages V_g, a field was established which led to a negative polarization of the films in contact with the insulating SiO_2. Such a polarization leads to an increase of the electron concentration or a decrease of the defect-electron concentration in a given material. Since an increase of conductance was observed, electrons are characterized as the majority charge-carriers in Cl_4MePTCDI as well as in MePTCDI (not shown). Consistently, the opposite behavior, i.e. a decrease of I_d, was observed for negative V_g. The mobility of the electrons was calculated from the linear part of a plot of I_d in dependence on V_g as proposed by Horowitz [22] by using the transconductance g_m, where Z is the channel width, L the channel length, C_i the capacitance of the insulating layer and V_d the applied drain-voltage:

$$g_m = \left|\frac{\partial I_d}{\partial V_g}\right|_{V_d=\text{const.}} = \frac{Z}{L}\mu C_i V_d \qquad (1)$$

The specific conductivity σ for the films was calculated from the slope of the linear part in the plot of conductance vs. average film thickness. Using the obtained values of the mobility μ and σ, the charge-carrier concentration n was calculated from

$$n = \frac{\sigma}{e\cdot\mu} \qquad (2)$$

where e is the elementary charge. Typical values of σ, n and μ for thin films of both materials are listed in Table 2.

It can be seen that the specific conductivity of thin films of the planar MePTCDI is about 100 times higher compared to that of the twisted Cl_4MePTCDI due to different electronic coupling in the solid state. [2] The measured values for the mobility of MePTCDI were found in a similar range as those reported earlier for thin films of

[2] If looked at in more detail, an influence of film preparation conditions on σ and μ can be observed. A lower deposition rate led to an increased σ mainly caused by an increase in μ since n was almost constant. A decreased number of defects and grain boundaries in the films would explain this. Such an influence of deposition rate and substrate temperature on the size of molecular islands is well-known and an increased charge-carrier mobility was reported [35–41]. For MePTCDI the specific relevance of charge-carrier hopping across a disordered grain boundary as opposed to transport within a crystalline needle is obvious and leads to the large difference between the mobility in thin films (6×10^{-4} cm^2 V^{-1} s^{-1} in our experiments) and in single crystals ($\leqslant 1$ cm^2 V^{-1} s^{-1} for this class of materials [42]) or highly ordered liquid crystalline phases (up to 0.6 cm^2 V^{-1} s^{-1} [43]). For the amorphous Cl_4MePTCDI such strong structural differences can not be expected in grain boundaries and the mobility in thin films should be rather close to the bulk value so that the mobility in a MePTCDI single crystal can be assumed to be up to 10 000 times higher compared to the disordered Cl_4MePTCDI.

perylene-3,4,9,10-biscarboximide (2.9×10^{-5} $cm^2\,V^{-1}\,s^{-1}$ at 298 K) [23] and perylene-3,4,9,10-tetracarboxilic acid dianhydride (1.1×10^{-5} $cm^2\,V^{-1}\,s^{-1}$ at 303 K) [24]. Also the mobility for MePTCDI is found to be about 100 times higher compared to the Cl_4MePTCDI. For both materials a constant charge-carrier concentration of about 10^{18} cm^{-3} was calculated which indicated that about 1 molecule in 1000 (about 10^{21} molecules cm^{-3} for both materials) carried a charge-carrier and hence was reduced under the present experimental conditions, since electrons were detected to be the majority charge-carrier. This rather similar concentration of charge-carriers has to be expected in view of the similar positions of unoccupied electronic levels calculated from the UPS results. Such dopant reactions have been well established for molecular semiconductors [24–27]. Dopant molecules can be intentionally brought in contact with growing films [25,26], reactions can occur following film formation [27] or, as in the present study, dopant molecules unintentionally present in the preparation chamber serve to dope the films. Possible candidates for these reactions would be either fragments of the molecules from the evaporation step or constituents of the vacuum system's residual gas. Since it has to be assumed that MePTCDI and Cl_4MePTCDI would form quite different amounts of different fragments the similarity in n would be difficult to explain based on doping by fragments. It is therefore concluded that reducing gas molecules like CO (desorbing from the resistive heating coils) or H_2 (low pumping rate by turbomolecular pumps) present in the vacuum chamber at similar concentrations for both materials (same preparation chamber, same preparation conditions) were responsible for the observed doping reactions. This conclusion was also drawn earlier when a series of substituted phthalocyanines was studied and a clear correlation was seen between the binding energy of electronic levels and the observed conduction type [21,28].

3.4. Temperature-dependence of charge-carrier generation and mobility

In order to study the mechanism of conduction in the two materials the temperature-dependence of the specific conductivity, the Seebeck coefficient and the charge-carrier mobility were measured between room temperature and the sublimation temperature of the films. The specific conductivity showed Arrhenius-type characteristics. A thermal activation energy of the specific conductivity $E_A = 0.20\ \text{eV} \pm 0.01\ \text{eV}$ was found for MePTCDI and $E_A = 0.34\ \text{eV} \pm 0.01\ \text{eV}$ for Cl_4MePTCDI on both, microstructured or macroscopic electrodes, again in agreement with a stronger electronic coupling in MePTCDI compared with Cl_4MePTCDI.

The temperature-dependence of the charge-carrier mobility was measured on the microstructured interdigitated electrodes within a temperature range between 303 K and about 430 K for MePTCDI. An Arrhenius-behavior was found for lower temperatures. The linear regression gives a value of $E_H = 0.11$ eV for the thermal activation of the charge-carrier mobility. [3] From these values we estimate the thermal activation of the charge-carrier concentration by subtracting E_H from E_A (see Eq. (2)) of $\Delta E = 0.09 \pm 0.01$ eV. These values are in a good agreement with the values obtained earlier [13] (see Table 2), where thin films were investigated by measurements of conductance and thermoelectric power.

To measure the activation energy of the charge-carrier generation in Cl_4MePTCDI, measurements of the thermoelectric power were carried out for films deposited on substrates of quartz glass with 10 mm electrode distance. Negative values of the Seebeck coefficient S were obtained which prove the n-type semiconductivity of the sample. When

[3] For larger grains of MePTCDI, a deviation of the mobility at higher temperature from the Arrhenius characteristics (and other models) was found whereas smaller grains led to a typical Arrhenius-behavior. For large grains and hence a small number of grain boundaries the temperature dependence of μ should be dominated by changes within the crystalline needles of MePTCDI. The molecules along the a-axis [44] of the crystal show a small thermal expansion compared with the strong temperature dependence in the b–c plane [8]. A similar behavior was reported for phthalocyanines [45]. Within an a-stack, μ should be higher, so the rate limiting step would be the hopping from stack to stack. Since the separation of the a-stacks is increased at higher temperature, also the barrier for hopping from stack to stack is increased. This effect over-compensates the thermal activation expected for μ by the different models and therefore none of the models would fit $\mu(T)$ at higher temperature.

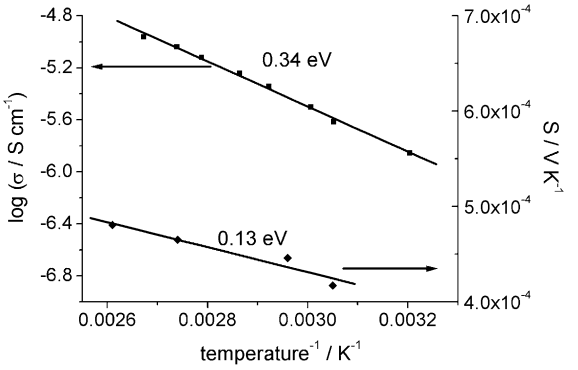

Fig. 6. Temperature dependence of the Seebeck coefficient and the specific conductivity of the Cl_4MePTCDI(2) (see Table 2) film. Values of the activation energies (E_A and ΔE) calculated from the slopes are shown in the graph.

plotted vs. $1/T$, S showed an Arrhenius-type thermal activation of the charge-carrier generation, as expected if conduction by one dominating type of charge-carrier is assumed [29]. The temperature-dependence of S and σ is compared in Fig. 6 (see also Appendix A). The linear regression of σ gives a value of $E_A = 0.34 \pm 0.01$ eV and that of S gives $\Delta E = 0.13 \pm 0.04$ eV for the activation energy of the charge-carrier generation. The difference of these two values gives an estimate of the activation energy of the mobility of about $E_H = 0.21 \pm 0.05$ eV. For films of Cl_4MePTCDI deposited on microstructured interdigitated electrodes an activation of the mobility (hopping energy) $E_H = 0.23$ eV was found in the Arrhenius plots. Subtracting these values from the activation energy of the specific conductivity ($E_{A,Cl_4MePTCDI} = 0.35$ eV) led to an activation energy of the charge-carrier generation of $\Delta E = 0.12$ eV in the case of the film Cl_4MePTCDI ($E_A = E_H + \Delta E$, see Eq. (2)). These values show a very good agreement (Table 2) with the value obtained from the thermoelectric power measurements. Consistency of the different experimental techniques is thereby shown, which also points at the fact that these parameters are characteristic for the material under the given preparation conditions since the samples are of widely differing geometry.

When the data are compared with the values reported for MePTCDI (see Table 2) the activation energy for the charge-carrier generation is found to differ less than the activation energy of the mobility among the two materials. The difference in the activation energy of the specific conductivity is therefore predominantly caused by the difference in the activation energy of the mobility.

4. Conclusions

Experimentally determined values of ΔE can be used for the calculation of the energetic position of the Fermi-level E_F relative to the level of conduction. As an estimate for the energy of the lowest unoccupied molecular orbitals (E_{LUMO}) the value calculated above from UPS and UV/vis absorption spectroscopy is used, which does not, however, consider differences in the exciton dissociation energy. A slightly higher dissociation energy estimated for Cl_4MePTCDI and the slightly larger frontier orbital gap of Cl_4MePTCDI compensate the lower HOMO position of this material and quite similar LUMO levels have to be expected for MePTCDI and Cl_4MePTCDI. The similar concentrations of charge-carriers in the materials originating from reactions with the same molecules of the residual gas (about one ionized molecule in 1000) can therefore be explained. Based on the assumption that the Fermi energy is located in the energetical center between the highest occupied and lowest unoccupied levels also at elevated temperature and that conduction occurs in the lowest unoccupied levels of the LUMO, values of E_F were calculated from the activation energy of the charge-carrier generation by using $E_F = E_{LUMO} - \Delta E/2$. Quite similar values of E_F were obtained for MePTCDI and Cl_4MePTCDI relative to the respective LUMO but also on an absolute scale which stands for the thermal generation of charge-carriers with a similar activation energy as observed in the experiments. Fig. 7 is a schematic representation of energy levels within MePTCDI and Cl_4MePTCDI. Effects caused by the energetic disorder found in the transport of charge-carriers in Cl_4MePTCDI are summarized in a Gaussian distribution of trap states (see Appendix A).

Due to the rather constant energetic conditions of the materials, the consequences of the different molecular structure and the resulting change in the

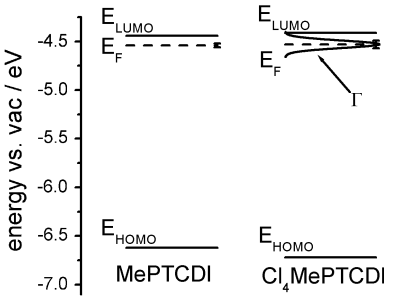

Fig. 7. Energetic positions of the HOMO, LUMO and the Fermi-level (E_F) of both materials. For E_F the error bar is shown as well as the Gaussian distribution according to the disorder formalism.

solid-state structure and film morphology of MePTCDI compared with Cl_4MePTCDI could be studied and the influence on the electric properties of thin films could be elucidated. The specific conductivity of the Cl_4MePTCDI with its low intermolecular interaction was found to be about 100 times lower compared with MePTCDI that showed a considerably larger coupling of the aromatic cores. This difference in conductivity was caused by a 100 times lower mobility of the charge-carriers for Cl_4MePTCDI. In the well-ordered MePTCDI the charge-carriers obviously move faster through the crystals, presumably supported by the strong and temperature-stable molecular stacks along the *a*-axis [8]. Hopping from one such stack to another is most likely limiting the mobility within the crystalline grains of MePTCDI. The hopping sites are distributed in a narrow range of energies and the temperature-dependence of the mobility should be described by the phonon-assisted hopping model. Within films of Cl_4MePTCDI, however, the limitation of the charge-carrier mobility is caused by the lower intermolecular interactions caused by the amorphous structure as well as by the geometrical bottle-neck of conduction pathways in grain boundaries.

Acknowledgements

The authors are grateful to N.R. Armstrong, K.W. Nebesny and P.A. Lee (University of Arizona, Tucson, AZ) for continuous support in the UPS analysis and its discussion, to D. Wöhrle (IOMC, University of Bremen) for helpful discussions and to K. Hesse (IAPC, University of Bremen) for help in the design of the electrical measurements as well as to U. Storm and J. Binder (IMSAS, University of Bremen) for developing and providing the microstructured substrates. Financial support by the State of Bremen (Matec 1.1) and the Deutsche Forschungsgemeinschaft (Schl 340/ 4-1, 4-2) is gratefully acknowledged.

Appendix A. Temperature-dependence of μ in thin films of amorphous molecular semiconductors (Cl_4MePTCDI)

In the Arrhenius plot of the conductivity of Cl_4MePTCDI a deviation from the linearity can be observed, pointing at a temperature dependence of E_H. Because of the small temperature range ($303 > T > 353$ K), this temperature dependence of the hopping energy could be omitted for the above comparison purposes but deserves a more rigorous treatment and this treatment may be also of interest in other examples of amorphous semiconductors in OFET structures. For amorphous thin films, a dependence of E_H on temperature has been observed in a number of time-of-flight experiments and the disorder formalism has been proposed [30] with an energetic disorder Γ assuming a Gaussian distribution and an off-diagonal, spatial disorder Σ to provide a good model for the temperature dependence of μ. The disorder formalism leads to a dependence of μ on the temperature as follows:

$$\mu = \mu_0 \exp\left(-\left(\frac{2\Gamma}{3kT}\right)^2\right) \times \exp\left(C\left(\left(\frac{\Gamma}{kT}\right)^2 - \Sigma^2\right)\sqrt{E}\right) \quad \text{(A.1)}$$

where μ is the mobility, μ_0 the mobility at infinite temperature and at zero field (ground mobility), C an empirical constant (2.9×10^{-4} V cm^{-1}) and $E(= V_d/L)$ the applied electric field in the direction of transport.

To adjust the disorder formalism to the need of an electrical field vertical to the direction of transport in measurements of the field-effect, (A.1) is inserted into (1), which leads to

$$g_m = \left|\frac{\partial I_d}{\partial V_g}\right|_{V_d=\text{const}} = \frac{Z}{L} C_i V_d \mu_0 \exp\left(-\left(\frac{2}{3}\frac{\Gamma}{kT}\right)^2\right) \times \exp\left(C\left(\left(\frac{\Gamma}{kT}\right)^2 - \Sigma^2\right)\sqrt{\frac{V_d}{L}}\right) \quad (A.2)$$

For the calculation of Γ , (A.2) is reorganized to

$$\ln g_m = \ln \mu_0 - C\Sigma^2\sqrt{\frac{V_d}{L}} - \ln\left(\frac{L}{ZC_iV_d}\right) + \left(C\sqrt{\frac{V_d}{L}} - \frac{4}{9}\right)\left(\frac{\Gamma}{kT}\right)^2 \quad (A.3)$$

that allows to determine Γ from the linear regression of a plot of $\ln g_m$ in dependence on T^{-2}.

For the calculation of Σ and μ_0, (A.2) was reorganized to

$$\ln\left(\frac{g_m}{V_d}\right) = \ln\left(\frac{Z}{L}C_i\mu_0\right) - \left(\frac{2}{3}\frac{\Gamma}{kT}\right)^2 + \left(C\left(\left(\frac{\Gamma}{kT}\right)^2 - \Sigma^2\right)\sqrt{\frac{V_d}{L}}\right) \quad (A.4)$$

and $\ln(g_m/V_d)$ is plotted against $\sqrt{V_d}$.

The results obtained for Cl_4MePTCDI are shown in Table 3 and are compared with values of μ for other perylene diimides reported from TOF-experiments.

The present results and the observed trends are consistent with those reported in the literature. For *N*,*N*′-bis(1,2-dimethylpropyl)-1,4,5,8-naphthalin-tetracarboxylic acid diimide (MePrNTCDI) [31] and *N*,*N*′-bis(2-diphenethyl)-3,4,9,10-perylene-tetracarboxylic acid diimide (PhEtPTCDI) [32] a higher mobility μ, a higher ground mobility μ_0 and a lower structural disorder Σ were reported than for Cl_4MePTCDI (present experiments) or 1,6,7,12-tetraphenoxy-*N*,*N*′-bis(2,6-diisopropyl-phenyl)-3,4,9,10-perylene-tetracarboxylic acid diimide (PhO_4-PrPhPTCDI) [33]. Based on experience with other *N*-substituted PTCDI [34] it can be assumed that the longer side chains in MePrNTCDI, PhEtPTCDI or PhO_4PrPhPTCDI led to a smaller intermolecular interaction compared with, e.g., MePTCDI. These materials were therefore successfully treated [31–33] in the disorder formalism of electric conduction and the small intermolecular interactions led to solubility of the pigments, as was also observed for Cl_4MePTCDI in the present experiments. The planar orientation of the aromatic cores of MePrNTCDI and PhEtPTCDI, however, still led to a higher intermolecular interaction in those materials when compared to Cl_4MePTCDI or PhO_4-PrPhPTCDI. Former work showed that the overlap of the aromatic core changed with the substitution at the imid nitrogen, but that the formation of stacks of the aromatic cores was still possible for planar molecules [34]. PhO_4PrPhPTCDI showed a low mobility comparable to that of Cl_4MePTCDI, caused by the similarity in the structure of the molecules which both carry a substituent in the bay-position of the aromatic core (four phenoxy-groups in the case of PhO_4PrPhPTCDI). The ground

Table 3
Mobility μ, ground mobility μ_0, energetic disorder Γ and spatial disorder Σ of Cl_4MePTCDI according to the disorder formalism for amorphous solids and comparable molecules

Material	μ/cm^2 V^{-1} s^{-1} (T/K)	Γ/eV	μ_0/cm^2 V^{-1} s^{-1}	Σ
Cl_4MePTCDI (1)	2.56×10^{-5} (303)	0.077	0.0077	2.29 ± 0.70
Cl_4MePTCDI (2)	7.44×10^{-6} (303)	0.088	0.0047	3.47 ± 0.30
MePrNTCDI[a]	1×10^{-4} (327)	0.093	0.01	2.3
PhEtPTCDI[a]	4.8×10^{-4}	0.080	0.011	1
PhO_4PrPhPTCDI[a]	10^{-5}	0.096	0.00053	

[a] MePrNTCDI: *N*,*N*′-bis(1,2-dimethylpropyl)-1,4,5,8-naphthaline-tetracarboxylicacid-diimide, PhEtPTCDI: *N*,*N*′-bis(2-diphenethyl)-3,4,9,10-perylene-tetracarboxylicacid-diimide, PhO_4PrPhPTCDI: 1,6,7,12-tetraphenoxy-*N*,*N*′-bis(2,6-diisopropylphenyl)-3,4,9,10-perylene tetracarboxylicacid-diimide.

mobility in $PhO_4PrPhPTCDI$, however, is about ten times lower than that in $Cl_4MePTCDI$ which can be explained by the larger substituents (phenoxy>Cl). These substituents should lead to a larger distance of the aromatic cores in the solid and hence to a further decrease of the hopping probability of charge-carriers.

References

[1] F. Garnier, Acc. Chem. Res. 32 (1999) 209.
[2] D. Wöhrle, D. Meissner, Adv. Mater. 3 (1991) 129.
[3] J.J.M. Halls, C.A. Walsh, N.C. Greenham, E.A. Marseglia, R.H. Friend, S.C. Moratti, A.B. Holmes, Nature 376 (1995) 498.
[4] C.J. Brabec, N.S. Sariciftci, J.C. Hummelen, Adv. Funct. Mater. 11 (2001) 15.
[5] N. Sato, H. Yoshida, K. Tsutsumi, J. Mater. Chem. 10 (2000) 85.
[6] H. Graaf, D. Schlettwein, N.I. Jaeger, Synth. Met. 109 (2000) 151.
[7] M. Sadrai, L. Hadel, R.R. Sauers, S. Husain, K. Krogh-Jespersen, J.D. Westbrook, G.R. Bird, J. Phys. Chem. 96 (1992) 7988.
[8] D. Schlettwein, H. Graaf, J.-P. Meyer, T. Oekermann, N.I. Jaeger, J. Phys. Chem. B 103 (1999) 3078.
[9] M. Sadrai, G.R. Bird, J.A. Potenza, H.J. Schugar, Acta Cryst. C 46 (1990) 637.
[10] D. Schlettwein, K. Hesse, H. Tada, S. Mashiko, U. Storm, J. Binder, Chem. Mater. 12 (2000) 989.
[11] U. Storm, Dissertation, Universität Bremen 2001.
[12] H. Graaf, D. Schlettwein, N.I. Jaeger, Phys. Chem. Chem. Phys. 1 (1999) 1801.
[13] J.-P. Meyer, D. Schlettwein, D. Wöhrle, N.I. Jaeger, Thin Solid Films 258 (1995) 317.
[14] D. Schlettwein, K. Hesse, N.E. Gruhn, P.A. Lee, K.W. Nebesny, N.R. Armstrong, J. Phys. Chem. B 105 (2001) 4791.
[15] H. Ishii, K. Sugiyama, S. Ito, K. Seki, Adv. Mater. 11 (1999) 605.
[16] I.G. Hill, A. Kahn, Appl. Phys. 86 (1999) 2116.
[17] R. Schlaf, B.A. Parkinson, P.A. Lee, K.W. Nebesny, N.R. Armstrong, J. Phys. Chem. B 103 (1999) 2984.
[18] A. Schmidt, N.R. Armstrong, personal communication.
[19] Y. Hirose, C.I. Wu, V. Aristov, P. Soukiassian, A. Kahn, Appl. Surf. Sci. 113/114 (1997) 291.
[20] H. Graaf, S. Forrest, in preparation.
[21] D. Schlettwein, in: H.S. Nalwa (Ed.), Supramolecular Photosensitive and Electroactive Materials, Academic Press, San Diego, 2001, p. 211.
[22] G. Horowitz, Adv. Mater. 10 (1998) 365.
[23] T. Suga, M. Iizuka, S. Kuniyoshi, K. Kudo, K. Tanaka, Synth. Met. 102 (1999) 1050.
[24] W. Böhm, T. Fritz, K. Leo, Phys. Stat. Sol. 160 (1997) 81.
[25] S. Hiller, D. Schlettwein, N.R. Armstrong, D. Wöhrle, J. Mater. Chem. 8 (1998) 945.
[26] M. Pfeiffer, A. Beyer, B. Plönnings, A. Nollau, T. Fritz, K. Leo, D. Schlettwein, S. Hiller, D. Wöhrle, Solar Energy Mater. Solar Cells 63 (2000) 83.
[27] J. Simon, J.-J. Andre, Molecular Semiconductors: Photoelectrical Properties and Solar Cells, Springer, Berlin, 1985.
[28] D. Schlettwein, N.R. Armstrong, J. Phys. Chem. 98 (1994) 11771.
[29] D. Emin, in: L.L. Kazmerski (Ed.), Polycrystalline and Amorphous Thin Films and Devices, Academic Press, London, 1980, p. 17.
[30] M. van der Auweraer, F.C. De Shryver, P.M. Borsenberger, H. Bässler, Adv. Mater. 6 (1994) 199.
[31] P.M. Borsenberger, W.T. Gruenbaum, E.H. Magin, Phys. Stat. Sol. (b) 190 (1995) 555.
[32] E.H. Magin, P.M. Borsenberger, J. Appl. Phys. 73 (1993) 787.
[33] P. Ranke, I. Bleyl, J. Simmerer, D. Haarer, A. Bacher, Appl. Phys. Lett. 71 (1997) 1332.
[34] G. Klebe, F. Graser, E. Hädicke, J. Berndt, Acta Cryst. B 45 (1989) 69.
[35] K. Reichelt, X. Jiang, Thin Solid Films 191 (1990) 91.
[36] S.R. Forrest, Chem. Rev. 57 (1997) 1793.
[37] J.-P. Meyer, Dissertation, Universität Bremen, 1997.
[38] D. Schlettwein, A. Back, T. Fritz, B. Schilling, N.R. Armstrong, Chem. Mater. 10 (1998) 601.
[39] C.D. Dimitrakopoulos, P.R.L. Malenfant, Adv. Mater. 14 (2002) 99.
[40] A. Facchetti, Y. Deng, A. Wang, Y. Koide, H. Sirringhaus, T.J. Marks, R.H. Friend, Angew. Chem. Int. Ed. 39 (2000) 4547.
[41] G. Horowitz, M.E. Hajilaoui, Adv. Mater. 12 (2000) 1046.
[42] N. Karl, Synth. Met. 133–134 (2003) 649.
[43] P.R.L. Malenfant, C.D. Dimitrakopoulos, J.D. Gelorme, L.L. Kosbar, T.O. Graham, Appl. Phys. Lett. 80 (2002) 2517.
[44] Cambridge Structural Data Base, 1999.
[45] J. Mizuguchi, G. Rihs, H.R. Karfunkel, J. Phys. Chem. 99 (1995) 16217.